J Fusion Energ (2015) 34:686–693
DOI 10.1007/s10894-015-9872-0

ORIGINAL RESEARCH

Comparison of Measured Soft X-Ray Yield Versus Pressure for NX1 and NX2 Plasma Focus Devices Against Computed Values Using Lee Model Code

P. Gautam · R. Khanal · S. H. Saw · S. Lee

Published online: 3 February 2015

Abstract The soft X-ray yield versus pressure curves of NX1 and NX2 plasma focus machines have been measured and published for different pressures and electrode configurations. In this work, the numerical experiments are carried out, using Lee model code. The Lee model code is configured for each of these devices NX1 and NX2 by fitting computed total discharge current waveform against a measured total discharge current waveform. The computed soft X-ray yield versus pressure curves are compared with the laboratory measured soft X-ray yield versus pressure data. The comparison shows agreement between computation and measurement of several important features of the yield versus pressure curves.

Keywords Plasma focus · Soft X-ray · Lee model code · Discharge current

Introduction

The dense plasma focus (DPF) is a coaxial gun, with the inner electrode (anode) electrically insulated from the outer electrode. After achieving a high vacuum condition, desired gas is admitted at a pressure of a few millibars. The plasma is produced when a capacitor bank is discharged through a low inductance transmission line into the machine. The discharge starts at one end of the electrodes and forms a current sheet flowing axisymmetrically between the anode and cathode. This current sheet is accelerated by the JXB force down the annular channel between the electrodes and entrains the ambient gas it encounters heating and compressing the resultant plasma in a thin sheet (or sheath). When the axisymmetric sheath reaches the end of the electrodes the axial motion changes into a radial motion as the current sheet implodes radially, eventually compressing the plasma into a high density high temperature column (the pinch).

The DPF produces abundant multi-radiation, a wide spectrum of photons and particles and is the subject of many studies and applications. From many devices and experiments large sets of data and information have been collected. For a long period of time after the discovery of DPF [1], most of the studies were done in hydrogen and its isotopes. For the past decades, significant potential applications of DPF as an intense (soft) X-ray source [2, 3] have been proposed and studied for example in the areas of microlithography and X-ray microscopy. Of importance to applications is the x-ray yield and the dependence of the yield on the plasma properties [4, 5].

The Plasma Focus emits both thermal (soft) as well as nonthermal (hard) X-rays but we will concentrate only on the thermal X-rays. The following electron–ion interaction processes are considered to be responsible for the thermal (soft) X-rays component: Bremsstrahlung (free–free transition) from the Coulomb interactions between electrons and ions; recombination (free bound transition) emission by an initially free electron as it loses energy on recombination

P. Gautam (✉) · R. Khanal
Central Department of Physics, Tribhuvan University, Kirtipur, Kathmandu, Nepal
e-mail: om.gautam49501@gmail.com

S. H. Saw · S. Lee
INTI International University, 71800 Nilai, Malaysia

S. H. Saw · S. Lee
Institute for Plasma Focus Studies, 32 Oakpark Drive, Chadstone VIC 3148, Australia

S. Lee
University of Malaya, Kuala Lumpur, Malaysia

with an ion; and line radiation or de-excitation emission (bound–bound transition) by the losses of energy when a bound electron falls to a lower ionic energy state. The Bremsstrahlung and recombination emission give rise to the continuum of the X-rays spectrum while the de-excitation process produces the characteristic line radiation of the plasma species. The relative strengths of the continuum and line emissions depend on how the plasma is formed [4–7]. The main mechanism of dominant hard X-rays production in plasma focus is moderately non-thermal high energy electrons striking the copper anode producing bremsstrahlung and characteristic radiation. The hard X-rays emission is correlated with neutron yield [4, 5].

The soft X-ray emitting source is the compressed (pinched) plasma column situated on the electrode axis at the open end of the electrode system in the vicinity of the anode face. The time integrated images show that it has roughly a cylindrical shape [8]. Our interest is to calculate the yield of the characteristic soft X-ray of a plasma focus operating in neon. For this purpose we use the Lee Model code.

The Lee code couples the electrical circuit with the dynamics of the plasma focus and its thermodynamics and radiation, enabling realistic simulation of all gross focus properties. The basic model (with axial and radial phases) described in 1984 [9], was successfully used to assist several experiments [10–14]. The radiation-coupled dynamics was included in a 5-phase code, which is successful to lead numerical experiments on radiation cooling [15]. In the 5-phase code, a reflected shock phase and a slow- compression radiative phase are added to the earlier model to simulate the X-ray emission from the plasma focus [16]. The signal-delay slug model was incorporated together with real gas thermodynamics and radiation-yield terms, which is so crucial to radial simulation. This development assisted other research projects [8, 17, 18] and was web-published in 2000 [19]. Plasma self-absorption was included [19] in 2007, improving soft X-ray yield simulation. The code has been used extensively as a complementary facility in several machines, such as; NX2 [8, 18, 20], UNU/ICTP PFF [12, 13, 15, 17, 21], NX1 [18], FMPF-3 [22], NX-3 [23], FN-II [24], PF-SY1 [7], PF-SY2 [25], DENA [26], GN1 [27], PF-160 [Dual Plasma Focus (DUPF)] [28], IR-MPF-100 [29]. It has also been used in other machines for their design and interpretation including ultra-miniature pinch PF discharge operating at 0.1 J nano-focus [30]. Information obtained includes axial and radial dynamics [13, 31, 32], SXR emission characteristics and yield [7, 17, 18, 33–36], design of machines [12, 13, 17, 18, 32–34, 36, 37], optimization of machines [13, 17, 18, 31, 33, 38] together with the adaptation of the Filippov-type DENA [26]. Plasma focus SXR yield calculations [7, 25, 34–37, 40], pinch current and SXR yield limitations [6, 39], optimization of SXR yield [7, 34–37], radiative collapse and cooling [41, 42], current stepped PF [43], PF neutron yield calculations [44, 45], current and neutron yield limitations [6, 46], neutron saturation [47, 48] and extraction of diagnostic data [49–52] and the anomalous resistance phase (RAN) data [53] from the current signals have been studied applying the code [54, 55]. Speed-enhanced PF [32] was facilitated. The inclusion of the neutron yield, Y_n, using beam target mechanism [44, 54–56] is one the great step in the development, incorporated in the versions [54, 55] of the code (later than RADPF5.13), resulting in realistic Y_n scaling with I_{pinch} [44, 47, 48]. The code has been used to develop scaling laws for soft X-rays [36, 57–60] and bench-mark numbers and scaling trends for ion beam flux, ion beam fluence, beam ion number, ion beam current, power flow density, and damage factor for all gases [61, 62]. Application of ion beam calculations to production of short-lived radioisotopes were made by Akel et al. [63]. The description, theory, code and a board range of results of this 'Universal Plasma Focus Laboratory Facility' are accessible for download from [54]. In this present work we use the code RADPF5.15de to look at the SXR yield as a function of operating pressures.

In the Lee model code [54, 55] neon line radiation Q_L is calculated as follows:

$$\frac{dQ_L}{dt} = -4.6 \times 10^{-31} n_i^2 Z Z_n^4 (\pi r_p^2) z_f \Big/ T \quad (1)$$

where, n_i is the number density, Z is the effective charge number, Z_n is the atomic number, z_f and r_p are the pinch length and pinch radius, respectively, and T is the plasma pinch temperature. Q_L can be obtained by the integration over the pinching period. At the temperatures of the interest in the experiments, the neon SXR yield $Y_{sxr} = Q_L$. The balance quantity after the reduction of the self-absorption is emitted as a soft X-ray. This effect is included in the Lee Code in the model calculation [54, 55].

Techniques for the Numerical Experiments

The Lee Model Code is first configured to work as one of the plasma focus by inputting the tube parameters a, b and z_0 together with the bank parameters L_0, C_0 and the stray resistance r_0 and the operating parameters V_0, P_0 and the gas fill. The tube parameter of the device shows the size of tube used in the plasma focus device, bank parameters shows the capacity of the inductor, capacitance and the resistance used in the combination of circuit of device and operational parameter are operating voltage and the pressure of gas used there. The standard practice to fit the total discharge current waveform to experimentally measured value is done by adjusting the four model parameters: axial mass swept-up factor (f_m), axial current factor (f_c), radial mass swept-up factor (f_{mr}) and radial plasma current factor

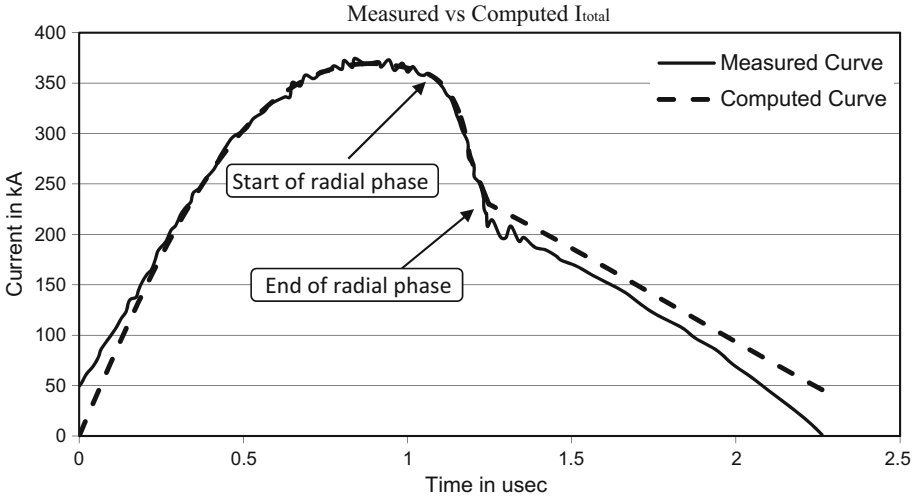

Fig. 1 Computed discharge current fitted to the published measured current for NX2 from Fig. 7 (b) of [64] at operating voltage 11.5 kV and pressure 3 torr and anode length of 5 cm. The fitting was done only up to the computed end of the radial phase as indicated in the waveform

(f_{cr}) [37, 54, 55]. It is seen and known that the current trace of the focus is the best indicator of the gross performance of the focus device. Important information like axial and the radial phase dynamics and the essential energy transfer are quickly visible from the current trace, which shows the importance of fitting of the current trace [54].

The Numerical Experiments With NX2

Fitting the Computed Current Trace to Obtain the Model Parameters

Lee et al. [61–63] have published various works with laboratory measurements from the NX2, including information and a typical current waveform on soft X-ray yield at a typical pressure of 4 mbar (i.e. 3 torr) with 5 cm anode operated at 11.5 kV and also with pressure 2.6 torr with 5 cm anode operated with 11 kV [35]. We first fit the computed current waveform to the published measured waveform of [64] Fig. 7(b).

We configure the Lee code (version RADPF5.15de) to operate as the NX2 starting with the following published bank and tube parameters extracted from Table no. 5.2 of [66] and Fig. 3 of [64]:

Bank parameters	$L_0 = 11.5$ nH	$C_0 = 28.8$ μF	r_0 = not given
Tube parameters (cm)	b = 4	a = 1.9	$z_0 = 5$
Operating parameters	$V_0 = 11.5$ kV	$P_0 = 3$ torr Neon	

where, L_0 is the static inductance, C_0 is the storage capacitance, b is the tube outer radius, a is the inner radius, z_0 the anode length, V_0 the operating voltage and P_0 the operating initial pressure.

The numerically computed total discharge current waveform is fitted to the measured by adjusting the model parameters f_m, f_c, f_{mr} and f_{cr} one by one until the numerically computed waveform agrees with measured waveform. First, to adjust the rising slope and the rounding off the peak current the axial model parameters fm and fc are adjusted and then to adjust the computed slope and depth of the dip the radial parameters fmr and fcr are fitted. This process is case sensitive in that if any bank parameter such as L_0 or C_0 is not correctly given, no good fit is obtainable (which affect all results in plasma dynamics).

To obtain a reasonably good fit in case of NX2 the following bank and tube parameters (L_0, C_0, z_0 and r_0) have to be used with slight adjustments to b;

Bank parameters	$L_0 = 15$ nH	$C_0 = 28$ μF	$r_0 = 2.5$ mΩ
Tube parameters (cm)	b = 4.1	a = 1.9	$z_0 = 5$
Operating parameters	$V_0 = 11.5$ kV	$P_0 = 3$ torr Neon	
Together with the model parameters		$f_m = 0.1$	$f_c = 0.7$
		$f_{mr} = 0.14$	$f_{cr} = 0.69$

Moreover the current calibration factor of the measured current waveform is adjusted so that the measured peak current is corrected to that of the computed peak current. This is because the code is charge-consistent, hence given a known initial charge stored in the capacitor bank, once the discharge waveform is correctly fitted to the measured waveform, the peak current is unambiguously computed. Hence the computed peak is the correct value and is used to re-calibrate the measured current peak value.

The fitted computed current waveform is compared with the published waveform in Fig. 1, which shows good

agreement and the two traces are inseparable at the regions of interest from axial to radial phase up-to the computed end of current dip. The measured waveform does show a further dip of some 20 kA. This extended dip of 20 kA is small compared to the computed dip of 130 kA; and the overall fit is considered to be acceptable. We thus conclude that the model parameters for this plasma focus in this regime of operation have been correctly obtained.

Computing the Soft X-ray Yield as a Function of Operating Pressure

The code is configured to operate as the NX2 using the bank and tube parameters mentioned above and using the fitted model parameters. Numerical experiments are then carried out at various initial pressures for neon gas. The soft X-ray yields for the various pressures are then tabulated in Table 1.

The computed yields recorded in Table 1 are then plotted in Fig. 2 together with the measured yield curve obtained from the published source [64] with more details from Fig. 6.68 of [66].

Figure 2 shows several features of reasonable agreement between the numerical and experimental values. The code gives the optimum soft X-ray yield at 4.1 torr with a value of 27.7 J; whereas the experimentally measured soft X-ray yield peaks at 3.5 torr with a value of 20 J. The shape of the computed yield curve is also very similar to the measured yield curve although the computed yield curve appears to fall off a little more sharply on each side of the yield peak than the measured yield curve. An analysis of the data given in [66] indicates that the uncertainty in the yield measurement is around 20 % at the 20 J level (i.e. 4 at 20 J) and there is also the uncertainty in the pressure measurement of around 0.2 Torr. Moreover there is fluctuation of yield from shot to shot which would increase the uncertainty of each of the measured points. It could be estimated that these fluctuations could typically add another 20 % to the uncertainty in each of the yield measurements. Taking this into account the computed and measured yield versus pressure curves can be considered to be in good agreement. It is noted that the code only requires the waveform of the current trace and that by fitting the computed waveform to the measured waveform adjusting only four model parameters fm, fc, fmr, fcr. Once the fitting is completed so that the computed current waveform reasonably agrees with the measured current waveform, the code outputs a reasonable soft X-ray yield and a computed yield versus pressure curve in good agreement with the measured yield versus pressure curve.

Table 1 Computed Ysxr as functions of pressure; together with some computed pinch properties for NX2

Po Torr	Ipeak kA	Ipinch start kA	Tpinch max 10^6	Axialpeak va cm/us	Radialpeak vs cm/us	Radialpeak vp cm/us	rmin cm	zmax cm	Pinch duration dur ns	Vmax kV	ni pinchmax (10^23)/m^3	EINP %	SF	Yline (Ysxr) J/shot
1.0	330	174	7.49	10.5	35.0	24.9	0.25	2.7	17.1	35.3	0.7	23.4	174	0.23
2.0	356	179	4.31	8.3	27.8	19.0	0.25	2.7	21.4	28.6	1.4	27.0	133	1.77
3.0	369	174	2.80	7.1	24.8	16.5	0.23	2.7	22.9	25.1	2.5	27.9	112	6.80
3.5	374	169	2.25	6.6	24.0	15.6	0.20	2.7	23.3	24.0	3.7	28.1	105	13.01
3.7	376	166	2.02	6.5	22.7	15.3	0.17	2.7	27.7	23.6	5.2	28.8	103	21.82
3.9	377	164	1.85	6.3	21.8	15.0	0.16	2.7	28.3	23.2	6.3	28.8	101	26.04
4.1	**379**	**161**	**1.70**	**6.2**	**20.9**	**14.6**	**0.16**	**2.8**	**29.3**	**22.6**	**7.0**	**28.6**	**98**	**27.66**
4.3	380	159	1.57	6.1	20.1	14.3	0.16	2.8	30.6	21.9	7.1	28.3	96	26.26
4.5	381	156	1.45	5.9	19.4	14.0	0.17	2.7	31.6	21.3	6.7	27.8	95	22.97
5.0	384	149	1.20	5.7	17.7	13.1	0.19	2.7	34.6	19.5	5.7	26.4	90	13.46
6.0	389	133	0.80	5.2	14.9	11.5	0.20	2.6	41.9	15.4	6.3	23.7	84	3.75
7.0	393	113	0.54	4.8	12.4	9.7	0.21	2.6	54.9	10.8	6.7	21.0	78	0.93

Bold numbers represent the values at 4.1 torr (maximum Ysxr yield)

Where, *SF* speed factor [12] in $kAcm^{-1}torr^{-1/2}$

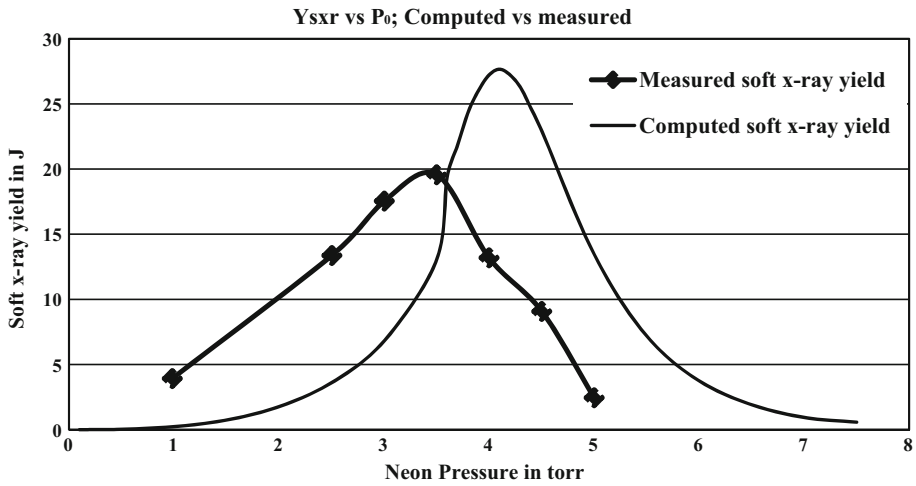

Fig. 2 Computed and the measured values from fig. no. 6.68 of [66] of Ysxr as function of P_0 for NX2 at operating voltage 11.5 kV

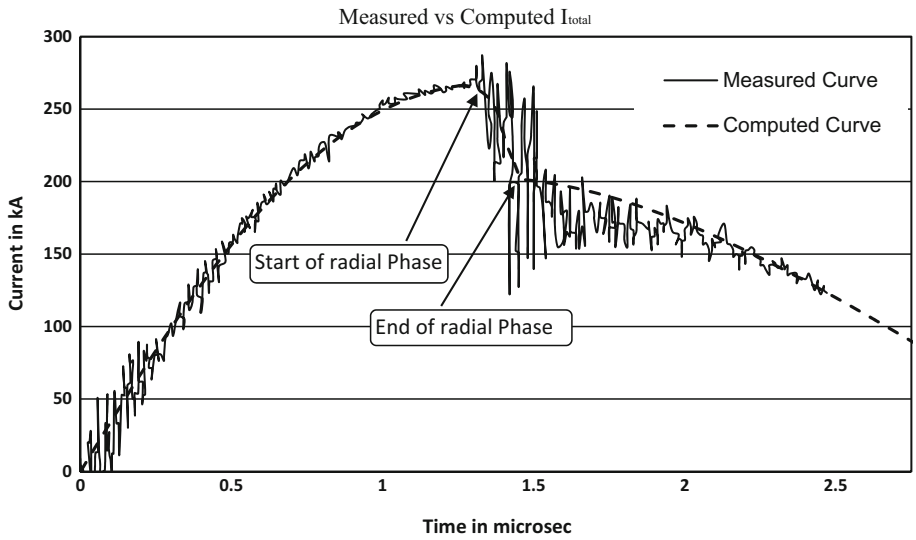

Fig. 3 Computed discharge current compared with the published measured current from Fig. 7(a) of [64] at operating voltage 10 kV and pressure of 5.3 torr with 3.5 cm anode

The Numerical Experiments With NX1

Fitting the Numerically Computed Current Trace to Obtain the Model Parameters

Lee et al. have published laboratory measurements from the NX1, including information and a typical current waveform on soft X-ray yield at a typical pressure of 7 mbar (5.3 torr) with 3.5 cm anode operated at 10 kV from page no. 190 of [66]. We first fit the computed current waveform to the published measured waveform found in [64] Fig. 7(a).

We configure the Lee code (version RADPF5.15de) to operate as the NX1, extracting the following configuration from our sources [64–66] primarily from Tables 6.11 and 6.12 and Fig. 6.4 of [66] pertaining to the published current waveform we are using:

Bank parameters	$L_0 = 29$ nH	$C_0 = 31$ μF	r_0 = not given
Tube parameters (cm)	$b = 5$	$a = 3$	$z_0 = 3.5$
Operating parameters	$V_0 = 10$ kV	$P_0 = 5.3$ torr Neon	

Table 2 Computed Ysxr as functions of pressure; together with some computed pinch properties for NX1

Po Torr	Ipeak kA	Ipinch start kA	Tpinch max 10^6	Axialpeak va cm/us	Radialpeak vs cm/us	Radialpeak vp cm/us	rmin cm	Zmax Cm	Pinch duaration dur ns	Vmax kV	ni pinchmax (10^23)/m^3	EINP %	SF	Yline (Ysxr) J/shot
2.0	244	151	5.99	6.8	30.9	21.6	0.22	2.6	17.7	33.3	0.9	17.4	91	0.33
4.0	263	158	3.47	5.4	25.6	17.0	0.21	2.5	20.3	29.3	1.9	20.2	69	2.52
6.0	269	154	2.25	4.6	23.3	15.3	0.17	2.5	21.2	28.2	4.6	21.4	58	11.32
7.0	271	151	1.81	4.3	20.9	14.5	0.13	2.5	24.1	27.5	8.3	22.1	54	21.94
7.2	**272**	**150**	**1.74**	**4.3**	**20.6**	**14.3**	**0.13**	**2.6**	**24.9**	**27.3**	**8.8**	**22.2**	**53**	**22.67**
7.4	272	149	1.68	4.2	20.2	14.1	0.13	2.5	25.0	27.0	8.9	22.0	53	21.98
8.0	273	147	1.50	4.1	19.0	13.7	0.14	2.5	26.6	26.2	8.6	21.6	51	18.64
10.0	276	137	1.06	3.7	16.1	12.3	0.17	2.5	31.1	22.9	7.2	19.4	46	6.30
12.0	278	125	0.75	3.4	13.5	10.6	0.17	2.5	38.7	18.5	9.0	17.3	42	2.10

Bold numbers represent the values at 7.2 torr (maximum Ysxr yield)

To obtain a reasonably good fit in case of NX1 the following bank and tube parameters (L_0, C_0, z_0 and r_0) have to be used:

Bank parameters	$L_0 = 29$ nH	$C_0 = 31$ μF	$r_0 = 3$ mΩ
Tube parameters (cm)	$b = 4.3$	$a = 1.9$	$z_0 = 3.5$
Operating parameters	$V_0 = 10$ kV	$P_0 = 5.3$ torr Neon	
Together with the model parameters		$f_m = 0.04$	$f_c = 0.7$
		$f_{mr} = 0.05$	$f_{cr} = 0.75$

It can be seen that the computed total discharge current waveform agrees with the published measured total current waveform at the regions of interest from axial and radial phase up-to the end of the pinch phase (Fig. 3).

Computing the Soft X-ray Yield as a Function of Operating Pressure

For the fitted model parameters, numerical experiments are then carried out at various pressures in neon. The soft X-ray yield is then tabulated in Table 2.

The computed yields are then plotted against pressure in Fig. 4 and compared with the measured values from Fig. 6a of [64] with more details from Fig. (6.65) of [66]. The comparison shows that the computed soft X-ray yield versus pressure curve agrees reasonably with the published measured curve in the same features as already found for the case of NX2 above.

The peak value of the computed soft X-ray yield vs pressure curve is 22.7 J at 7.2 Torr whereas the measured peak value of soft X-ray yield is 19 J operated at 9 Torr. Taking into account the error bars and the known shot-to-shot fluctuations that may be expected of plasma focus devices including the NX1, it may be considered that the computed yield versus pressure curve agrees well with the measured yield versus pressure curve for this case of the NX1.

Conclusion

The Lee Model Code is used to compute the soft X-ray yield versus pressure curve of the Singaporean plasma focus devices NX1 and NX2 with different design of electrode. The computed results agree reasonably well in;

(1) The trends of the soft X-ray yield versus pressure curve
(2) The maximum yield, and
(3) The optimum pressure value.

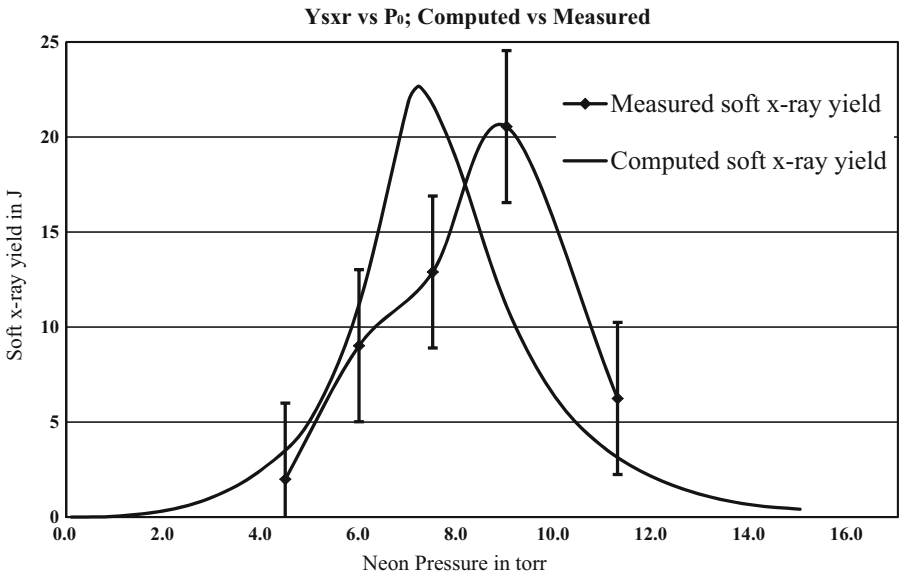

Fig. 4 Computed and the measured from Fig. 6.65 of [66] Ysxr as functions of P_0 for NX1 at operating voltage 10 kV

Tables 1 and 2 are presented for plasma dynamics and properties contributing to the soft X-rays. The results encourage us to use Lee Model Code for plasma focus devices with anodes of different shapes. For example the anode of NX2 is a straight cylinder with abrupt transition from the axial phase to the radial phase, whereas NX1 has an anode with a rounded shaper with gradual transition from the axial phase to the radial phase. Despite the differences, the code appears to give good agreement in both devices for neon soft X-ray yield versus pressure when compared with the measured graphs particularly when we consider the uncertainty inherent in the soft X-ray yield measurements in these experiments, and the typical shot-to-shot fluctuations of yields in these devices. It could be conjectured that the fitting of the computed current trace to the measured current trace produces model parameters which reflect also the differences in the anode shape.

References

1. J.W. Mather, Phys. Fluids **7**, S28 (1964)
2. Y. Kato, I. Ochiai, Y. Watanabe, S. Murayama, J. Vac. Sci. Technol. **B6**, 195 (1988)
3. W. Neff, J. Eberle, R. Holz, R. Lebert, F. Richter, SPIE **1140**, 1310 (1989)
4. M. Liu, "Soft X-rays from Compact Plasma Focus"; Ph.D. Dissertation, NIE, Nanyang Technological University, Singapore 2006
5. M. Favre, S. Lee, S.P. Moo, C.S. Wong, X-ray emission in a small plasma focus operating with H2-Ar mixtures. Plasma Sources Sci. Technol. **1**(2), 122 (1992)
6. S. Lee, S.H. Saw, Appl. Phys. Lett. **92**, 021503 (2008). doi:10.1063/1.2827579
7. M. Akel, Sh Al-Hawat, S.H. Saw, S. Lee, J. Fusion Energ. **29**, 223 (2010)
8. S. Bing, "Plasma dynamics and X-ray emission of the plasma focus"; Ph.D. Dissertation, NIE, Nanyang Technological University, Singapore 2000
9. S. Lee, in *Radiation in Plasmas Vol II*, ed. by B. McNamara. Process of Spring College in Plasma Physics (1983) (World Scientific Pub Co., ICTP, Trieste, Singapore, 1984), pp. 978–987
10. S. H. Saw; "Experimental Studies of a Current Stepped Z-Pinch"; Ph.D. Dissertation, University of Malaya, Kuala Lumpur, Malaysia 1990
11. S. Lee, IEEE Trans. Plasma Sci. **19**, 912 (1991)
12. S. Lee, A. Serban, IEEE Trans. Plasma Sci. **24**, 1101 (1996)
13. S. Lee et al., American. J. Phys. **56**, 62 (1988)
14. T.Y. Tou, S. Lee, K.H. Kwek, IEEE Trans. Plasma Sci. **17**, 311 (1989)
15. J. B. Ali; "Development and studies of a small plasma focus"; Ph.D. Dissertation, Universiti Teknologi Malaysia, Malaysia 1990
16. M. H. Liu, S. Lee, ICPP and EPS Conf. on Contr. Fusion Plasma Phys. ECA **22(C)** 2169 (1998)
17. M.H. Liu, X.P. Feng, S.V. Springham, S. Lee, IEEE Trans. Plasma Sci. **26**, 135 (1998)
18. S. Lee, P. Lee, G. Zhang, X. Feng, V.A. Gribkov, M. Liu, A. Serban, T. Wong, IEEE Trans. Plasma Sci. **26**, 1119 (1998)
19. S. Lee, http://ckplee.myplace.nie.edu.sg/plasmaphysics/ (2000/2007)
20. D. Wong, P. Lee, T. Zhang, A. Patran, T.L. Tan, R.S. Rawat, S. Lee, An improved radiative plasma focus model calibrated for neon-filled NX2 using a tapered anode. Plasma Sources Sci. Technol. **16**(1), 116 (2007)
21. S. Lee; Twelve years of UNU/ICTP PFF-a review, Abdus Salam ICTP, http://eprints.ictp.it/31/ (1998)
22. Rishi Verma, R.S. Rawat, P. Lee, S.V. Springham, T.L. Tan, Fusion Energ. **32**, 2–10 (2013). doi:10.1007/s10894-012-9517-5
23. R. Verma, R.S. Rawat, P. Lee, A.T.L. Tan, H. Shariff, G.J. Ying, S.V. Springham, A. Talebitaher, U. Ilyas, A. Shyam, IEEE Trans. Plasma Sci. **40**(12), 3280–3289 (2012). doi:10.1109/TPS.2012.2220569
24. F. Castillo, J.J.E. Herrera, J. Rangel, J.A. Alfaro, M.A. Maza, V. Sakaguchi, Braz. J. Phys. **32**, 3–12 (2002)
25. M. Akel, Sh Al-Hawat, S.H. Saw, S. Lee, J. Fusion Energ. **29**, 94 (2010)

26. V. Siahpoush, M.A. Tafreshi, S. Sobhanian, S. Khorram, Plasma Phys. Control. Fusion **47**, 1065 (2005)
27. A. Singh, S. Lee, S.H. Saw, Int. J. Mod. Phys. Conf. Ser. **32**, 1460325 (2014)
28. S.H. Saw, V. Damideh, P.L. Chong, P. Lee, R.S. Rawat, S. Lee, Int. J. Mod. Phys. Conf. Ser. **32**, 1460322 (2014)
29. S.T. Ong, K. Chaudhary, J. Ali, S. Lee, Plasma Phys. Control. Fusion **56**, 075001 (2014)
30. C. Pavez, L. Soto, IEEE Trans. Plasma Sci. **38**, 5 (2010)
31. S. Lee, IEEE Trans. Plasma Sci. **19**, 5 (1991)
32. A. Serban, S. Lee, Plasma Sour. Sci. Technol. **6**, 78 (1997)
33. S.H. Saw, M. Akel, P.C.K. Lee, S.T. Ong, S.N. Mohamad, F.D. Ismail, N.D. Nawi, K. Devi, R.M. Sabri, A.H. Baijan, J. Ali, S. Lee, J. Fusion Energ. **31**, 411 (2012)
34. S.H. Saw, P.C.K. Lee, R.S. Rawat, S. Lee, IEEE Trans. Plasma Sci. **37**, 1276 (2009)
35. S. Lee, R.S. Rawat, P. Lee, S.H. Saw, J. Appl. Phys. **106**, 023309 (2009)
36. S.H. Saw, S. Lee, Energ. Power Eng. **2**, 65 (2010)
37. M. Akel, S. Lee, S.H. Saw, IEEE Trans. Plasma Sci. **40**, 3290 (2012)
38. S.P. Moo, C.K. Chakrabarty, S. Lee, IEEE Trans. Plasma Sci. **19**, 515 (1991)
39. M. Akel, S. Lee, J Fusion Energ. **32**, 107 (2013)
40. M. Akel, S. Lee, J Fusion Energ. **31**, 122 (2012)
41. S. Lee, S.H. Saw, J. Ali, J. Fusion Energ. **32**, 42 (2013)
42. M. Akel, S. Lee, J Fusion Energ. **32**, 111 (2013)
43. S. Lee, S.H. Saw, J. Fusion Energ. **31**, 603 (2012)
44. S. Lee, S.H. Saw, J. Fusion Energ. **27**, 292 (2008)
45. S. Lee, S.H. Saw, L. Soto, S.V. Springham, S.P. Moo, Plasma Phys. Control. Fusion **51**, 075006 (2009)
46. S. Lee, P. Lee, S.H. Saw, R.S. Rawat, Plasma Phys. Control. Fusion **50**, 065012 (2008)
47. S. Lee, Plasma Phys. Control. Fusion **50**, 105005 (2008)
48. S. Lee, Appl. Phys. Lett. **95**, 151503 (2009)
49. S. Lee, S.H. Saw, P.C.K. Lee, R.S. Rawat, H. Schmidt, Appl. Phys. Lett. **92**, 111501 (2008)
50. S.H. Saw, S. Lee, F. Roy, P.L. Chong, V. Vengadeswaran, A.S.M. Sidik, Y.W. Leong, A. Singh, Rev. Sci. Instrum. **81**, 053505 (2010)
51. S. Lee, S.H. Saw, R.S. Rawat, P. Lee, R. Verma, A. Talebitaher, S.M. Hassan, A.E. Abdou, M. Ismail, A. Mohamed, H. Torreblanca, S. Al-Hawat, M. Akel, P.L. Chong, F. Roy, A. Singh, D. Wong, K. Devi, J. Fusion Energ. **31**, 198 (2012)
52. S.H. Saw, R.S. Rawat, P. Lee, A. Talebitaher, A.E. Abdou, P.L. Chong, F. Roy, J. Ali, S. Lee, IEEE Trans. Plasma Sci. **93**, 3813 (2013)
53. S. Lee, S.H. Saw, A.E. Abdou, H. Torreblanca, Characterizing plasma focus devices—role of the static inductance—instability phase fitted by anomalous resistances. J. Fusion Energ. **30**(4), 277–282 (2011)
54. S Lee, Radiative Dense Plasma Focus Computation Package: RADPF http://www.intimal.edu.my/school/fas/UFLF/File1RADPF.htmhttp://www.plasmafocus.net/IPFS/modelpackage/File1RADPF.html (archival websites)
55. S. Lee, J. Fusion Energ. **33**, 319 (2014)
56. V.A. Gribkov et al., J. Phys. D Appl. Phys. **40**, 3592 (2007)
57. S. Lee, S.H. Saw, P. Lee, R.S. Rawat, Plasma Phys. Control. Fusion **51**(10), 105013 (2009)
58. S. Lee, S.H. Saw, Energies: special edition on "Fusion Energy". Energies **3**, 711–737 (2010). doi:10.3390/en3040711
59. S.H. Saw, S. Lee, Int. J. Energ. Res. **35**, 81 (2011). doi:10.1002/er.1758
60. S. Lee, S.H. Saw, Int. J. Energ. Res. **36**, 1366–1374 (2012). doi:10.1002/er.1918
61. S. Lee, S.H. Saw, Plasma focus ion beam fluence and flux—scaling with stored energy. Phys. Plasmas **19**, 112703 (2012)
62. S. Lee, S.H. Saw, Plasma focus ion beam fluence and flux—for various gases. Phys. Plasmas **20**, 062702 (2013). doi:10.1063/1.4811650
63. M. Akel, S.A. Salo, Sh Ismael, S.H. Saw, S. Lee, Phys. Plasmas **21**, 072507 (2014)
64. S. Lee, P. Lee, G.X. Zhang, V.A. Gribkov, X. Feng, M.H. Liu, A. Serban, IEEE Trans. Plasma Sci. **26**, 4 (1998)
65. S. Lee, P. Lee, G.X. Zhang, X. Feng, A. Serban, M.H. Liu, T.K.S. Wong, C. Selvam, A. Thang, Proc. SPIE **3183**, 277 (1997)
66. Z. Guixin, "Plasma soft X-ray source for microelectronic lithography," Ph.D. Dissertation, Nanyang Technological University, Singapore 1999